Available online at www.sciencedirect.com
SCIENCE DIRECT
Chemical Physics Letters 419 (2006) 269–272
CHEMICAL PHYSICS LETTERS
www.elsevier.com/locate/cplett

Electroluminescent properties of device based on ZnS:Tb/CdS core-shell nanocrystals

Ruinian Hua [a,*], Jinghua Niu [b], Mingtao Li [b], Tianzhi Yu [b], Wenlian Li [*,b]

[a] College of Life Science, Dalian Nationalities University, Dalian Economic Development Area, Liaoning Province, Dalian 116600, People's Republic of China
[b] Key Laboratory of Excited State Processes, Changchun Institute of Optics, Fine Mechanics and Physics, Chinese Academy of Sciences, Changchun 130033, People's Republic of China

Received 26 September 2005; in final form 23 November 2005
Available online 13 December 2005

Abstract

ZnS:Tb/CdS core/shell nanocrystals (NCs) were synthesized by reverse micelle method, and with a core crystal diameter of 3.0 and a 0.5 nm thick CdS shell and used as an electroluminescent material. Electroluminescent (EL) devices having a hybrid organic/inorganic multilayer structure were fabricated. Electron–hole recombination was confined at the ZnS:Tb/CdS NCs layer. Three emissions peaked at 440 nm form ZnS host, 546 nm ($^5D_4$–$^7F_5$) and 577 nm ($^5D_4$–$^7F_4$) of Tb^{3+} center were observed when the hybrid EL device at a bias of 13 V. The maximum luminance of the ZnS:Tb/CdS NCs-based reached 19 cd/m^2 at 25 V.

1. Introduction

Nanometer-sized semiconductor clusters have attracted growing interest during last decade [1,2], therefore, they have become an important class of luminescent materials because of the flexibility to the control optical and electronic properties by changing only the size of the materials. Generally, they exhibit strong size-dependent optical properties, i.e., an observed increased energy gap, which leads to a blueshift in the absorption feature with the decreasing particle sizes. This effect occurs when the size of the NCs is smaller than the corresponding bulk Bohr exciton radius, as a result of quantum confinement effect due to localization of charge carriers [3].

ZnS is a wide-gap (~3.6 eV) II–VI compound semiconductor material and is commercially used as a phosphor and also in thin-film electroluminescent (EL) devices. Since Bhargava et al. have given the first report on remarkable optical properties of Mn-doped ZnS NCs that were prepared by a room temperature chemical process in 1994 [4,5], and then a large amount of the investigations on semiconductor NCs has been focused on the photoluminescent (PL) properties of Mn [2,6–11], Cu [7,12], Sm [1,13], Tb [1,14], and Eu [3,15–19] doped ZnS NCs prepared by different techniques. For many purposes, epitaxially grown core/shell semiconductor nanocrystals, for which a wider band gap material is deposited to the core with a narrower band gap have been studied extensively [20]. As a result, both the electron and the hole are mostly confined in the core region. The photoluminescence quantum yield and stability can be greatly improved if compared with the plain core nanocrystals. Meanwhile several groups have attempted to fabricate another core/shell structure, where a material with narrower band gap was overgrown onto the core with wider band gap [21]. A few papers have also reported on the EL devices using undoped [22,23] or nano-semiconductor doped with transition metallic ions such as Mn^{2+} [24–26], and Cu^+ [27], respectively. Most of the nanocrystal-based EL devices consist of a hybrid organic/inorganic structure, where either an organic conjugated polymer and inorganic nanocrystal component exist as a separate layer or nanocrystals are embedded in a conjugated polymer matrix. Emissions from both PVK due to charge carriers recombination and ZnS:Mn NCs layer through impact excitation of Mn luminescent centers were

* Corresponding author.
E-mail address: rnhua@dlnu.edu.cn (R. Hua).

0009-2614/$ - see front matter © 2005 Elsevier B.V. All rights reserved.
doi:10.1016/j.cplett.2005.11.092

observed in the organic/inorganic hybrid device fabricated by PVK and ZnS:Mn NCs [25]. The EL properties of rare earth (RE) ions doped ZnS NCs have, however, never been reported. In this work, ZnS:Tb/CdS NCs sized about 4 nm were synthesized by reverse micelle method, and its EL performances was studied for the first time. The hybrid EL device with structure of indium tin oxide (ITO)//poly (3,4-ethylene-dioxythiophene)/poly (styrenesulfonate) (PEDOT-PSS)//poly (*N*-vinylcarbazole) (PVK)//ZnS:Tb/CdS NCs//2,9-dimethyl-4,7-diphenyl-1,10-Phenan-throline (BCP)//LiF//Al was constructed.

2. Experimental

ZnS:Tb/CdS core-shell nanocrystals were prepared via a reverse micelle method. In this method, $Zn(CH_3COO)_2 \cdot 2H_2O$, $TbCl_3 \cdot 6H_2O$, $LiCl \cdot H_2O$, $Na_2S \cdot 9H_2O$, and $Cd(CH_3COO)_2 \cdot 2H_2O$ were used for preparation of ($Zn^{2+} + Tb^{3+} + Li^+$)-, S^{2-}-, and Cd^{2+}-containing standard aqueous solutions. Each aqueous solution was stirred with dioctylsulfosuccinate, sodium salt (AOT)/heptane solution, forming the micellar solution. Tb-doped ZnS core nanocrystals were formed by mixing ($Zn^{2+} + Tb^{3+} + Li^+$)- and S^{2-}-containing micellar solutions rapidly for 15 min. LiCl was added since Li^+ on a Zn^{2+} site can serve as charge compensator for Tb^{3+} ions on Zn^{2+} sites [1]. For growth of a CdS shell layer, Cd^{2+}-containing micellar solution is added at a very slow rate (2 mL/min) into the ZnS:Tb core nanocrystal micellar solution (while maintaining a surplus of S ions to support CdS shell growth). In this reverse micelle route, the concentrations of Zn^{2+} and Cd^{2+} ions in water are 0.1 and 0.065 mol/L, respectively. Also the concentrations of water and AOT in heptane are 1 and 0.1 mol/L, respectively, The molar ratios of water-to-surfactant (w) are 10 for formation of ZnS:Tb core nanocrystals and 20 for the CdS shell layer. The Tb solution concentration in ZnS is 5 mol%. After addition of the Cd^{2+} micellar solution for 10 min, the resulting solution was then transferred into 100 mL stainless Teflon-lined autoclave and heated at 160 °C for 6 h. The resulted powders were collected and washed for several times with methanol and distilled water, respectively. Finally, the ZnS:Tb/CdS core-shell NCs were obtained after the samples were centrifuged (8000 rpm, 30 min) and dried in a vacuum at room temperature.

The hybrid EL device consisting of ITO//PEDOT-PSS (70 nm)//PVK (100 nm)//ZnS:Tb/CdS NCs (120 nm)//BCP (30 nm)//LiF (1 nm)//Al (100 nm) was constructed. PEDOT-PSS, PVK and ZnS:Tb/CdS NCs layers were prepared on the ITO-coated glass substrate by successive spin-coating. After dried in a vacuum oven at 80 °C for 40 min, the sample was loaded into vacuum chamber, where BCP, LiF and Al contact were deposited by thermal evaporation at a pressure of 5.0×10^{-4} Pa.

Nanocrystal size and morphology were measured using a JEM-2010 transmission electron microscopy (TEM) operated at 200 kV for imaging and direct determination of crystal size. The structure of the nanocrystals was characterized by X-ray powder diffraction (XRD) with a Japan Rigaku D/max-IIB diffraction with Cu $K\alpha_1$ radiation ($\lambda = 0.1541$ nm). PL spectra were measured using a Hitachi F-4500 fluorescence spectrometer. EL emission spectra were collected by a fiber optic and dispersed onto a CCD Si-detector.

3. Results and discussion

The XRD pattern of ZnS:Tb/CdS NCs was shown in Fig. 1. It is revealed that the crystals exhibit zinc-blende crystal structure. The three diffraction peaks are corresponding to (1 1 1), (2 2 0), and (3 1 1) planes of the cubic crystalline ZnS, respectively. Due to the size effect, the XRD peaks broaden and their widths become large as the crystals become smaller. For ZnS:Tb/CdS NCs, the XRD peaks intensity become weakly being the CdS shell exist. From the XRD analysis, no characteristic peaks of impurity phases were observed. The average sizes of ZnS:Tb/CdS NCs were calculated from the Debye–Scherrer equation to be around 3 nm. A typical TEM image (Fig. 2) show that the average size of the ZnS:Tb/CdS NCs is about 4 nm, indicating the CdS shell thickness of 0.5 nm. The size calculated from the XRD reflects only the ZnS:Tb core, since Peng et al. [28] demonstrated that the shell layer does not affect the XRD peak width from the core in a CdSe/CdS core/shell structure.

Fig. 3 shows the typical PL of the ZnS:Tb/CdS NCs and EL spectra of device based on core-shell ZnS:Tb/CdS NCs. The PL spectra of ZnS:Tb/CdS core-shell NCs excited by 379 nm are composed of six peaks located at 450, 466, 489, 543, 583, and 619 nm, respectively, and the peaks at 450 and 466 nm resulted from the ZnS/CdS host [1], and the other four sharp bands peaked at 489, 543, 583, and 619 nm are due to $^5D_4$–$^7F_6$, $^5D_4$–$^7F_5$, $^5D_4$–$^7F_4$, and $^5D_4$–$^7F_3$ electron transitions of Tb^{3+} ions, respectively [14]. When the EL device

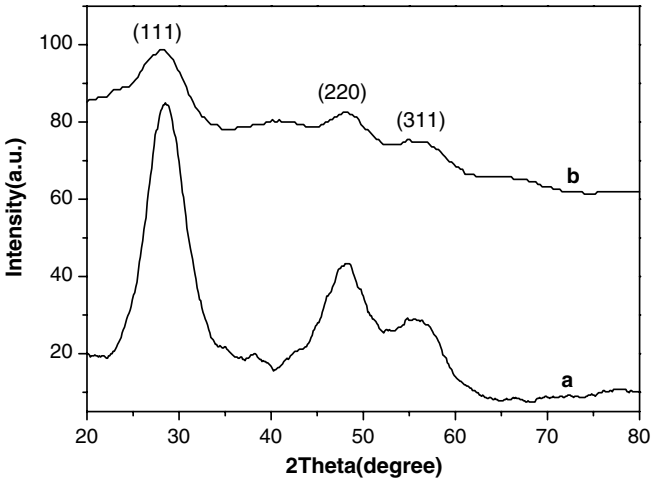

Fig. 1. XRD pattern of ZnS:Tb NCs (a) and ZnS:Tb/CdS NCs (b).

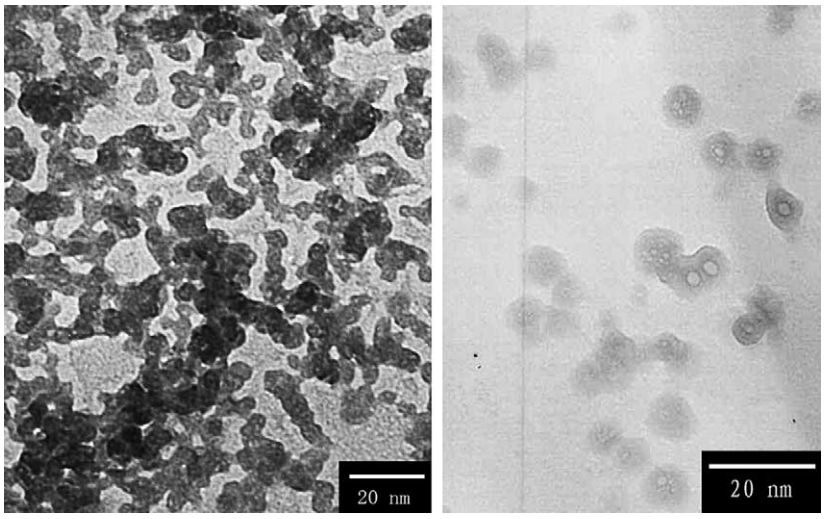

Fig. 2. TEM micrograph showing ZnS:Tb NCs (left) and ZnS:Tb/CdS core-shell NCs (right).

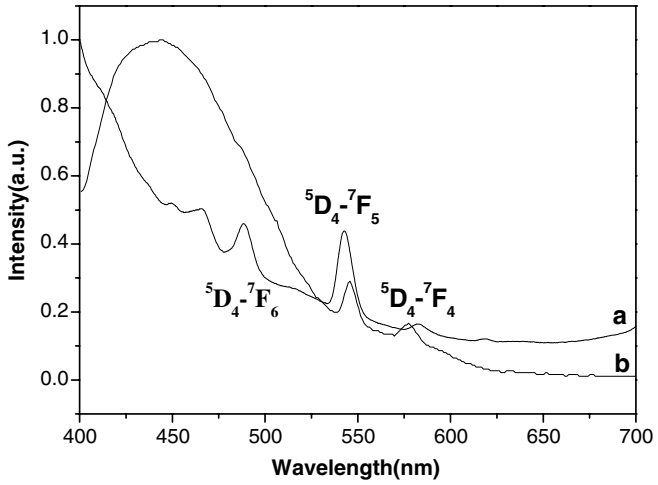

Fig. 3. Comparison of PL emission spectra from ZnS:Tb/CdS core-shell NCs ($\lambda_{exc} = 379$ nm) and EL emission spectra obtained from an ITO//PEDOT-PSS//PVK//ZnS:Tb/CdS NCs//BCP//LiF//Al device.

based on ZnS:Tb/CdS core-shell NCs was driven bias of 13 V, three peaks located at 440 from the ZnS host, 546 nm ($^5D_4$–$^7F_5$), and 577 nm ($^5D_4$–$^7F_4$) from Tb^{3+} center were observed. The peak should locate at 489 nm ($^5D_4$–$^7F_6$) from Tb^{3+} center, which was covered with the peak of ZnS host. The EL emission intensity slightly increased with increasing applied voltage, but in emission wavelength was not any changed because of the device decays faster. In the absence of the PEDOT-PSS layer, no noticeable EL emission was observed, indicating that the PEDOT-PSS layer would play important role for lowering the energy barrier for hole injection from the ITO electrode to PVK layer and so that increasing carrier recombination in the ZnS:Tb/CdS core-shell NCs layer. Most NCs-based EL devices using a conjugated polymer as a hole transport material show emission from both the NCs and polymer layer due to electron–hole recombination in both components [24,26]. In this work EL emission from PVK polymer is, however, not observed from our ITO//PEDOT-PSS//PVK//ZnS:Tb/CdS NCs//BCP//LiF//Al device, showing that only the ZnS:Tb/CdS core-shell NCs layer contributes to EL emission and because hole blocking role of the BCP layer the carrier recombination was confirmed to in the ZnS:Tb/CdS layer. According to above EL processes, energy-level diagram of device with ITO//PEDOT-PSS//PVK//ZnS:Tb/CdS NCs//BCP//LiF//Al is shown in Fig. 4 [26,27]. The band gap energy of ZnS nanocrystals with 3 nm is about 4.2 eV, which is much larger than that of macrocrystalline ZnS (3.6 eV) due to the quantum size effect. The energy barrier of 0.8 eV for the hole injection at the PEDOT-PSS/PVK interface would lead a high turn-on voltage and a low flowing current. The holes and electrons injected to the ZnS:Tb/CdS core-shell NCs layer through the PVK and BCP layer, respectively, and recombination to form the excitons on NCs ZnS host, then the excitons energy was transferred to the energy levels of the Tb^{3+} to achieve the characteristic emission of Tb^{3+}. The EL emission wavelength peaked at 546 nm was shifted to lower energy compared to its PL

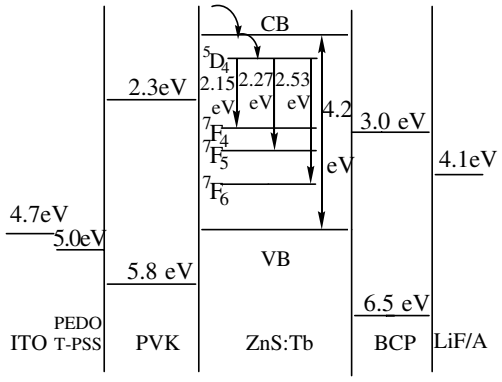

Fig. 4. Energy-level diagram of an ITO//PEDOT-PSS//PVK//ZnS:Tb/CdS NCs//BCP//LiF//Al device.

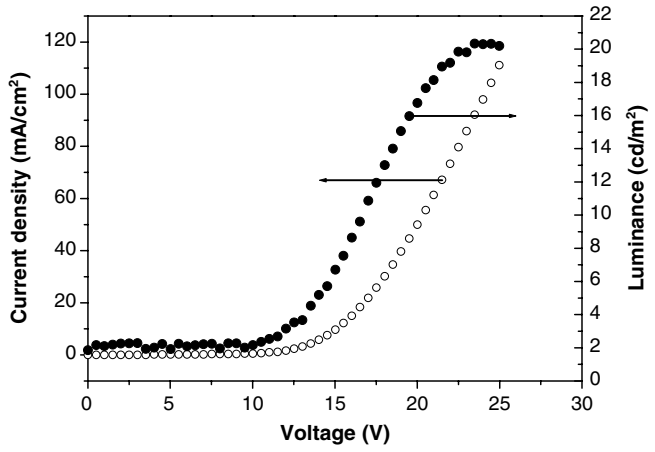

Fig. 5. Current density–voltage–luminance characteristics of the ITO//PEDOT-PSS//PVK//ZnS:Tb/CdS NCs//BCP//LiF//Al device.

spectrum, indicating that local heat effect from the large current and poor thermal conductivity of the emitting layer [27]. The current density–voltage–luminance characteristics of the ITO//PEDOT-PSS//PVK//ZnS:Tb/CdS NCs//BCP//LiF//Al device is showed in Fig. 5. It can be seen that the threshold of the device is about 13 V, suggesting that the main voltage drop occurred at the ZnS:Tb/CdS core-shell NCs layer. The result further confirms that the ZnS:Tb/CdS NCs layer controls the current density–voltage characteristic of the device. The maximum luminance of the ZnS:Tb/CdS core-shell nanocrystals-based device is about 19 cd/m^2 at 25 V.

4. Conclusion

In summary, ZnS:Tb/CdS core-shell NCs with a core crystal diameter of 3.0 nm and a shell thickness of 0.5 nm was synthesized by the reverse micelle method. Hybrid electroluminescent devices with a multilayer structure were fabricated using ZnS:Tb/CdS core/shell nanocrystals and conjugated polymer PVK. EL device composed of ITO//PEDOT-PSS//PVK//ZnS:Tb/CdS NCs//BCP//LiF//Al was tested. The three peaks located at 440 (ZnS host lattice excitation), 546 ($^5D_4$–$^7F_5$), and 577 nm ($^5D_4$–$^7F_4$) were observed when the hybrid device was driven at the direct current voltage of 13 V, and it was confirmed that the EL emission is from the ZnS:Tb/CdS core-shell NCs layer. The hybrid EL emission of the device resulted from f to f electron transition of Tb^{3+} ions which is from energy of exciton by recombination of the holes and electrons carried PVK host through energy transfer from PVK to the ZnS NCs host. EL device based the RE activated NCs ZnS can show obviously EL emission under bias driving although its turn-on voltage is also relative high and the stability will further be improved. Further experimental work is needed to the working mechanism of the device based on RE-ZnS/CdS core-shell NCs need to understand so that new material system and new structure device will be designed. It will be believed that many kinds of rare earth ions doped NCs semiconductor/polymer hydride organic devices would be fabricated.

Acknowledgements

This work was supported by the National Science Research Project foundation of China (No. 90201012) and the Postdoctoral Fund of Dalian Nationalities University (20056110).

References

[1] A.A. Bol, R. Beek, A. Meijerink, Chem. Mater. 14 (2002) 1121.
[2] R.S. Kane, R.E. Cohen, R. Silbey, Chem. Mater. 11 (1999) 90.
[3] S.C. Qu, W.H. Zhou, F.Q. Liu, N.F. Chen, Z.G. Wang, H.Y. Pan, D.P. Yu, Appl. Phys. Lett. 80 (2002) 3605.
[4] R.N. Bhargava, D. Gallagher, T. Welker, J. Lumin. 60–61 (1994) 275.
[5] R.N. Bhargava, D. Gallagher, X. Hong, A. Nurmikko, Phys. Rev. Lett. 72 (1994) 416.
[6] T. Igarashi, T. Isobe, M. Senna, Phys. Rev. B 56 (1997) 6444.
[7] S.J. Xu, S.J. Chua, B. Liu, L.M. Gan, C.H. Chew, G.Q. Xu, Appl. Phys. Lett. 73 (1998) 478.
[8] M. Tanaka, J. Qi, Y. Masumoto, J. Lumin. 87–89 (2000) 472.
[9] T. Kezuka, M. Konishi, T. Isobe, M. Senna, J. Lumin. 87–89 (2000) 418.
[10] B. Xia, I.W. Lenggoro, K. Okuyama, Chem. Mater. 14 (2002) 4969.
[11] T. Kubo, T. Isobe, M. Senna, J. Lumin. 99 (2002) 39.
[12] P. Yang, M. Lu, D. Xu, D. Yuan, G. Zhou, Chem. Phys. Lett. 336 (2001) 76.
[13] T. Kushida, A. Kurita, M. Watanabe, Y. Kanematsu, K. Hirata, N. Okubo, Y. Kanemitsu, J. Lumin. 87–89 (2000) 466.
[14] M. Ihara, T. Igarashi, T. Kusunoki, K. Ohno, J. Electrochem. Soc. 147 (2000) 2355.
[15] K. Swiatek, M. Godlewski, D. Hommel, Phys. Rev. B 42 (1990) 3628.
[16] D.D. Papakonstantinou, J. Huang, P. Lianos, J. Mater. Sci. Lett. 17 (1998) 1571.
[17] L. Sun, C. Yan, C. Liu, C. Liao, D. Li, J. Yu, J. Alloys Compd. 275–277 (1998) 234.
[18] W. Chen, J. Malm, V. Zwiller, Y. Huang, S. Liu, R. Wallenberg, J. Bovin, Phys. Rev. B 61 (2000) 11021.
[19] W. Chen, J. Malm, V. Zwiller, R. Wallenberg, J. Bovin, J. Appl. Phys. 89 (2001) 2671.
[20] J.J. Li, Y.A. Wang, W. Guo, J.C. Keay, T.D. Mishima, M.B. Johnson, X. Peng, J. Am. Chem. Soc. 125 (2003) 12567.
[21] X. Zhong, R. Xie, Y. Zhang, T. Basche, W. Knoll, Chem. Mater. 17 (2005) 4043.
[22] V.L. Colvin, M.C. Schlamp, A.P. Alivisatos, Nature 370 (1994) 354.
[23] B.O. Dabbousi, M.G. Bawendi, O. Onitsuka, M.F. Rubner, Appl. Phys. Lett. 66 (1995) 1316.
[24] X. Yang, X. Xu, Appl. Phys. Lett. 77 (2000) 797.
[25] H. Yang, P.H. Holloway, B.B. Ratna, J. Appl. Phys. 93 (2003) 586.
[26] H. Yang, P.H. Holloway, J. Phys. Chem. B 107 (2003) 9705.
[27] J. Huang, Y. Yang, S. Xue, B. Yang, S. Liu, J. Shen, Appl. Phys. Lett. 70 (1997) 2335.
[28] X. Peng, M.C. Schlamp, A.V. Kadavanich, A.P. Alivisatos, J. Am. Chem. Soc. 119 (1997) 7019.